Description of the yrast traps at very high angular momenta

Ploszajczak, M; Faessler, Amand; Leander, G; Nilsson, Sven Gösta

Published in:
Nuclear Physics, Section A

1978

1.D.2

Nuclear Physics **A301** (1978) 477–496;

DESCRIPTION OF THE YRAST TRAPS AT VERY HIGH ANGULAR MOMENTA

M. PLOSZAJCZAK †

Institut für Kernphysik, Kernforschungsanlage Jülich, D-5170 Jülich, West Germany

AMAND FAESSLER ††

State University of New York at Stony Brook, Stony Brook, NY 11794, USA

and

G. LEANDER and S. G. NILSSON

Lund Institute of Technology, Lund, Sweden

Received 17 June 1977

(Revised 16 March 1978)

Abstract: A microscopic description of yrast traps is given. The method is based on Hartree-Fock (HF) trial wave functions and a many-body Hamiltonian with a quadrupole-quadrupole (QQ) and a hexadecapole-hexadecapole (HH) force. The method is applied to study yrast traps in the beginning of the rare-earth region in highly neutron deficient nuclei where calculations suggest rotation around the symmetry axis: (i) The hexadecapole deformation at very high spin states is an important degree of freedom. It affects strongly the formation of yrast traps. (ii) Isomeric states at the yrast line are found up to angular momentum $I = 40\hbar$.

1. Introduction

The very high spin states in nuclei were first studied by Cohen, Plasil and Swiatecki [ref. [1])] in the classical liquid drop model. The physical implications of these results have been discussed by Bohr and Mottelson [2]). They predicted the existence of long-lived isomers at very high spin along the yrast line which are now usually called yrast traps. These may arise due to the fact that no collective rotation is possible around a symmetry axis.

Quantal calculations for the deformation energy surface at very high spin in the framework of the Strutinsky method have been performed at Dubna [3,4]), Lund-Warsaw [5,6]) and Jülich [7]). The work at Dubna and Lund-Warsaw uses a modified-oscillator (MO) potential which leads, due to the l^2 term, to difficulties with the value of the average moment of inertia. This difficulty is removed in the work from Jülich [7]) by employing a Woods-Saxon potential. In addition deformation energy surfaces

† Permanent address: Institute of Nuclear Physics, Radzikowskiego 152, 31-342 Cracow, Poland.
†† Permanent address: Institut für Kernphysik, Kernforschungsanlage Jülich, D-5170 Jülich, West Germany.

at very high spin have also been calculated using a two-body interaction [8-10]).

The yrast traps are connected with the energy gain due to the maximisation of the overlap of the nucleonic wave function by alignment (MONA effect [10])). Detailed analyses of the known two-particle spectra performed by Schiffer [11]) and by Molinari *et al.* [11]) show that the effective two-body interaction is strongly attractive for 0° and 180° angles between the two single-particle angular momenta for non-identical particles. In these cases the single-particle wave functions have the largest overlap. In contrast, for the relative angle 90° one has only a small overlap between the nucleonic wave functions and, consequently, the interaction is quite weak. As a consequence of these features of the two-body forces, the nucleus in the ground state of even-even nuclei is paired. For higher angular momenta the overlap between the nucleonic wave functions decreases leading to the increase of the excitation energy. Overlap of the single-particle wave functions increases once again for the aligned configurations and we gain (in these configurations) energy. This mechanism may be responsible for stabilizing the rotation around a symmetry axis, which is a condition for the existence of yrast traps. We shall see that MONA prefers negative deformations at the beginning of a shell, where particles are aligned, and it favours rotation around a symmetry axis of a positive deformed shape at the end of the shell at high spin states where holes are aligned.

This effect is included in a microscopic description but also in the Strutinsky approach if the single-particle energies are determined self-consistently. Since at least in principle this is the case, both methods should describe this effect (although the smoothing procedure will give in practice different results). The very similar results obtained in the Strutinsky approach [3-7, 12]) and this work seem to support this assumption.

The purpose of this work is twofold: First we give here a microscopic description based on the cranking Hartree-Fock theory for the formation of the yrast traps. Further we know that for the description of the ground-state properties hexadecapole deformation plays an important role. Therefore, *a priori* there is no reason to discard it for the calculations at high spins. Moreover, quadrupole deformation at high spins varies substantially and one might expect a similar behaviour for the hexadecapole deformations. Thus, we intend to analyze the effect of the hexadecapole deformation on the structure of the yrast line. For this purpose, our calculations include the Y_{40} component consistently in the trial wave function as well as in the many-body Hamiltonian. The calculations reported here have been performed only along the $\gamma = -60°$, $\beta_2 > 0$ line favoured by the classical LDM energy (i.e. the oblate nucleus rotating around the symmetry axis). However, the proposed description can be applied to any kind of rotation of the axially symmetric nucleus around the symmetry axis.

The details of the model formulations relevant to the present calculations are given in sect. 2. In this section we also discuss the essential ingredients of the existing

mechanisms to explain the yrast traps. In sect. 3, we show the results of the calculations for the neutron deficient rare earth nuclei $^{148}_{62}$Sm, $^{150}_{64}$Gd, and $^{158}_{70}$Yb. In these nuclei the lowest minimum of the total energy obtained using either the Strutinsky approach [5,6]) or the microscopic model of ref. [9]) corresponds to $\gamma = -60°$ for the angular momenta $I = 30$–$50\hbar$. For each nucleus we show the excitation energy of the states along the yrast line as well as the quadrupole and hexadecapole moments. Finally, in sect. 4, we summarize the main results of our work and give the conclusions.

2. Theory

We describe the nucleus at very high angular momenta using in principle a cranked Hartree-Fock theory. For the two-body residual interaction, the quadrupole-quadrupole and hexadecapole-hexadecapole forces are used. The trial wave function parametrized by the deformations β_2, γ, β_{40} is a Slater determinant built by cranked MO single-particle functions. The total energy of the system for a given angular momentum I has been obtained by minimising the sum of the Coulomb energy and the expectation value of the many-body Hamiltonian with respect to the deformation parameters.

2.1. HAMILTONIAN

We construct the trial wave function with the help of the model Hamiltonian:

$$H_t = \sum_{\tilde{a}\tilde{b}} \langle \tilde{a}|h|\tilde{b}\rangle C^+_{\tilde{a}} C_{\tilde{b}} - \omega_J \sum_{\tilde{a}\tilde{b}} \langle \tilde{a}|j_x|\tilde{b}\rangle C^+_{\tilde{a}} C_{\tilde{b}} - \sum_{\tilde{a},\tilde{b}>0} G_{\tau\tilde{a}}\delta_{\tau\tilde{a}\tau\tilde{b}} C^+_{\tilde{a}} C^+_{-\tilde{a}} C_{-\tilde{b}} C_{\tilde{b}}, \tag{1}$$

where the single-particle Hamiltonian h is defined as

$$h = h_0 - \hbar\omega_0 \alpha_\tau^2 r^2 \{\beta_2 \cos\gamma Y_{20} + \sqrt{\tfrac{1}{2}}\beta_2 \sin\gamma (Y_{22} + Y_{2-2}) + \beta_{40} Y_{40}\} \tag{2}$$

in which h_0 is the spherical single-particle energy term and β_2, β_{40} and γ are the deformation parameters. The basis states are chosen to be the eigenstates of the $\exp(i\pi J_x)$ operator and single-particle Hamiltonian h. They are defined as

$$\begin{aligned} |\tilde{a}\rangle &= \sqrt{\tfrac{1}{2}}(|a\rangle + \varphi_a|\bar{a}\rangle), \\ |-\tilde{a}\rangle &= \sqrt{\tfrac{1}{2}}\varphi_a(|a\rangle - \varphi_a|\bar{a}\rangle), \end{aligned} \tag{3}$$

with the phase $\varphi_a = (-1)^{l_a - \Omega_a + \frac{1}{2}}$. The shell-model states $|a\rangle$ and $|\bar{a}\rangle$ are written as

$$\begin{aligned} |a\rangle &= |\tau n l j \Omega\rangle_a, \\ |\bar{a}\rangle &= (-1)^{l_a + j_a - \Omega_a}|a\rangle. \end{aligned} \tag{4}$$

Such a basis proposed independently by Faessler *et al.* [8]) and by Goodman [13]) allows one to decouple the HFB equations. In the calculation of the trial wave function for the very high angular momentum states ($I \gtrsim 30\hbar$) we assume the pairing interaction to be zero. We get the trial wave function by diagonalizing in the basis consisting of the s.p. states in six oscillator shells, namely $N = 2$–7 for protons and $N = 3$–8 for neutrons. The trial Slater determinants contain wave functions of this diagonalization corresponding to $N = 4, 5$ for proton wave functions and $N = 5, 6$ for neutron wave functions in the spherical limit. This allows one to extend the model to higher deformations and angular momenta. But it is still limited to $\beta \leqq 0.4$–0.5 and $J \leqq 60\hbar$. Since we need it here only for $\beta \leqq 0.3$ and $J \leqq 40\hbar$, the present approximation seems to us satisfactory. The spherical single-particle energies entering the Hamiltonian h_0 are obtained from the MO version of the spherical shell model with the parameters (κ and μ for the $\boldsymbol{l} \cdot \boldsymbol{s}$ and l^2 terms) taken from ref. [14]). The eigenvalues ε_{Nlj} of H_{MO} ($\beta = 0$) for the proton shells $N = 4, 5$ and for the neutron shells $N = 5, 6$ are replaced by the spherical single-particle energies given by Kumar and Baranger [15]). Kumar and Baranger adapted the spherical single-particle energies to experimental data. Thus we do not expect to have difficulties with a too large moment of inertia for spins below $I = 60$ in which we are interested here. Higher shells (for example the $j_{15/2}$ neutron level) for which we used the l^2 term, do not play a role in the determination of the moment of inertia below angular momentum 60 as shown in ref. [7]). The values of single-particle energies ε_{Nlj} in other remaining shells are given relative to the state assumed to be at zero energy in the $N = 4$ proton shell and $N = 5$ neutron shell.

The quantities α_τ in eq. (2) are introduced [15]) in order to ensure equal radii for protons and neutrons

$$\alpha_\tau = \begin{cases} (2Z/A)^{1/3} & \text{for protons} \\ (2N/A)^{13/3} & \text{for neutrons.} \end{cases} \tag{5}$$

The cranking term $-\omega j_x$ forces the nucleus to rotate around the x-axis with the angular frequency ω_J. This frequency is determined from the condition

$$\langle \beta_2, \beta_{40}, \gamma, \omega | J_x | \beta_2, \beta_{40}, \gamma, \omega \rangle = \sqrt{J(J+1) - \langle J_z^2 \rangle}. \tag{6}$$

The coupling between the shells N and $N \pm 2$ given by the $r^2 Y_{\nu\mu}$ term in the Hamiltonian (1) has been included in the trial wave function. This coupling produces a significant change of the s.p. wave function for larger deformations β_2 and β_{40}.

In this case, many levels from the high-lying oscillator shells come close to the states near the Fermi level. Consequently, the states from different oscillator shells mix strongly and change their structure. In the total wave functions we have omitted all the single-particle wave functions which in the limit of $\beta_2 = 0$, $\beta_{40} = 0$ do not correspond to the oscillator shells $N = 4, 5$ for protons and $N = 5, 6$ for neutrons. It is possible to specify these levels as a function of β_2 and β_{40}, because the eigenvalues of the Hamiltonian (1) specified by the same good quantum numbers: isospin τ,

parity π and projection m onto the symmetry axis do not cross at any deformation. Such a choice of the s.p. wave functions has the advantage that a simple separable quadrupole-quadrupole force for the two-body interaction can still be used. It has been shown by Kumar and Baranger [15]) that the matrix elements of the quadrupole-quadrupole interaction approximate correctly the matrix elements of the "realistic" forces if one uses only those s.p. states available in two neighbouring shells for protons and neutrons. Within the considered group of s.p. states in our model, the change of the s.p. wave function with the deformation is properly taken into account. But it is also obvious that the extension of the model to large deformations and large angular momenta should not be trusted. According to test calculations we would expect that it is valid up to $\beta \leqq 0.4$ to 0.5 and $J \leqq 60\hbar$.

The many-body Hamiltonian consistent with the trial wave function obtained from the model Hamiltonian (1) can be written as:

$$\begin{aligned}\hat{H} = & \sum_{\tilde{a}} \varepsilon_{\tilde{a}} C_{\tilde{a}}^{+} C_{\tilde{a}} - \sum_{\tilde{a},\tilde{b}>0} G_{\tau_{\tilde{a}}} \delta_{\tau_{\tilde{a}}\tau_{\tilde{b}}} C_{\tilde{a}}^{+} C_{-\tilde{a}}^{+} C_{-\tilde{b}} C_{\tilde{b}} \\ & - \tfrac{1}{2} \sum_{\substack{\tilde{a}\tilde{b} \\ \tilde{c}\tilde{d} \\ \tau}} \chi_2 \alpha_{\tau_{\tilde{a}}} \alpha_{\tau_{\tilde{b}}} \sum_{\mu} \langle \tilde{a}|Q_{\mu}^{(2)}|\tilde{c}\rangle \langle \tilde{b}|(-1)^{\mu} Q_{-\mu}^{(2)}|\tilde{d}\rangle C_{\tilde{a}}^{+} C_{\tilde{b}}^{+} C_{\tilde{d}} C_{\tilde{c}} \\ & - \tfrac{1}{2} \sum_{\substack{\tilde{a}\tilde{b} \\ \tilde{c}\tilde{d} \\ \tau}} \chi_4 \alpha_{\tau_{\tilde{a}}} \alpha_{\tau_{\tilde{c}}} \langle \tilde{a}|Q_0^{(4)}|\tilde{c}\rangle \langle \tilde{b}|Q_0^{(4)}|\tilde{d}\rangle C_{\tilde{a}}^{+} C_{\tilde{b}}^{+} C_{\tilde{d}} C_{\tilde{c}},\end{aligned} \tag{7}$$

where

$$Q_{\mu}^{(\nu)} \equiv \hat{r}^2 Y_{\nu\mu}.$$

Here the $\varepsilon_{\tilde{a}}$ are the spherical single-particle energies as described before. χ_2 and χ_4 are the strengths of the quadrupole-quadrupole and hexadecapole-hexadecapole interactions and G_{τ} is the strength of the monopole pairing interaction. The self-consistency requirement for the trial wave function and the Hamiltonian (7) is given by

$$\begin{aligned}\beta_2 \cos\gamma &= \frac{\chi_2}{\hbar\omega} \sum_{\tau} \alpha_{\tau} \langle Q_0^{(2)} \rangle_{\tau}, \\ \beta_2 \sin\gamma &= \frac{\chi_2}{\hbar\omega} \sum_{\tau} \alpha_{\tau} \langle Q_2^{(2)} \rangle_{\tau}, \\ \beta_4 &= \frac{\chi_4}{\hbar\omega} \sum_{\tau} \alpha_{\tau} \langle Q_0^{(4)} \rangle_{\tau}.\end{aligned} \tag{8}$$

Here $\langle Q_{\mu}(\nu)\rangle$ are the expectation values of the quadrupole $Q_{\mu}^{(2)}$ ($\mu = 0,2$) and hexadecapole $Q_0^{(4)}$ moments. For $\omega_J = 0$ the minimum of the expectation value of the many-body Hamiltonian (7) with respect to β_2, γ, $\beta_{40}(\Delta_n, \Delta_p)$, along with the self-consistency condition (8) gives a Hartree-Fock-Bogoliubov (HFB) minimum for

the Hamiltonian (7). This statement is true provided that the exchange terms in the quadrupole and the hexadecapole interactions as well as the contribution of pairing force to the HF potential and the contribution of quadrupole and hexadecapole forces to the pairing potentials can be neglected. It has been argued in ref. [15]) that both assumptions are valid for the P+QQ Hamiltonian. For $\omega \neq 0$ one expects that those arguments hold in similar quality.

A further problem in this model is connected with the use of the quadrupole and hexadecapole forces as the residual interaction. With regard to the comparative values of the quadrupole matrix elements for the particles in the two shells under consideration we know from the work of Kumar and Baranger [15]) that the matrix elements between the states in the upper shell are too large compared with those calculated between the states in the lower shell. In order to overcome this difficulty, it has been proposed in ref. [15]) to include only a part of the upper shell or to scale all the quadrupole matrix elements of the upper shell with a factor which ensures the same rms radius. Since we want to describe in our model deformations up to $\beta = 0.4$ or 0.5 and angular momenta $J < 60\hbar$ (although we need only deformations $\beta \leqq 0.3$ and $J \leqq 40\hbar$ in this work), the completeness of the second shell must be considered to be important. The s.p. states included in the trial wave function obtained by diagonalizing the model Hamiltonian (1) contain for large deformations β_2 and β_{40} significant admixtures of the high-N states. Therefore we have to calculate the diagonal as well as the off-diagonal matrix elements of the $\hat{r}^2$ operator. The prescription we have used to scale the matrix elements of $\hat{r}^2$ is

$$r^2_{N\,iNj} = \left(\frac{N_0^\tau + \frac{3}{2}}{N_j^\tau + \frac{3}{2}}\right)^{\frac{1}{2}} \langle N_j^\tau | \hat{r}^2 | N_i^\tau \rangle \left(\frac{N_0^\tau + \frac{3}{2}}{N_i^\tau + \frac{3}{2}}\right)^{\frac{1}{2}}, \tag{9}$$

where

$$N_0^\tau = \begin{cases} 4 & \text{for protons} \\ 5 & \text{for neutrons.} \end{cases}$$

For small deformations $\beta \leqq 0.2$ which play the dominant role in this work our approach used for the radial matrix elements is identical with the one of Kumar and Baranger, since we selected for the calculations only those basis states which in the limit $\beta_2 = \beta_4 = 0$ correspond to the $N = 4, 5$ and $N = 5, 6$ shells for the protons and neutrons, respectively. For larger deformations ($\beta \approx 0.4$ to 0.5) for which other shells are admixed in our single-particle basis the above recipe simulates to keep effectively the $\Delta N = 2$ matrix elements equal to zero. [If one admixes higher or lower oscillator states one looses admixtures of the $N = 4, 5$ (for protons) and $N = 5, 6$ (for neutrons) oscillator states correspondingly in the single-particle basis. Eq. (9) guarantees that the radial matrix elements all have the same size.] It is known that the nuclear matter shows a large incompressibility, therefore for a deformed nucleus one should conserve the volume of the system [16,17]). In nuclear structure calculations with a realistic two-body nucleon-nucleon interaction the volume conservation

should come out automatically without any additional constraints. However, in the practical calculations with a model force like the pairing or quadrupole-quadrupole one, this condition is not fulfilled and one is forced to correct for this deficiency [9,10]). A simple approximate way to guarantee the volume conservation is the scaling of the oscillator length [9]). Thus the oscillator length is taken to be deformation dependent and has the form

$$b^2(\beta_2, \gamma, \beta_{40}) = \frac{\hbar}{m\omega(\beta_2, \beta_{40}, \gamma)}.$$

In this case the expectation value of the quadrupole-quadrupole force has to be multiplied by a factor $|b(\beta_2, \beta_{40}, \gamma)/b(0, 0, 0)|^4$. The influence of the volume conservation on the single-particle term of the Hamiltonian (7) is conceptually less clear. It is difficult to take into account this effect for the core particles not under consideration. It is, however, of minor importance because the deformation in this model is influenced mainly by the Coulomb and quadrupole-quadrupole forces.

The deformation energy surface for the angular momentum J is written as:

$$E^J(\beta_2, \beta_{40}, \gamma, \Delta_n, \Delta_p) = \langle \beta_2, \beta_{40}, \gamma, \Delta_n, \Delta_p, J|\hat{H}|\beta_2, \beta_{40}, \gamma, \Delta_n, \Delta_p, J\rangle + E_{\text{Coul}}(\beta_2, \beta_{40}, \gamma) \tag{10}$$

where $\hat{H}$ is the many-body Hamiltonian given in eq. (7). For the calculations of the energy landscapes for $I \gtrsim 30\hbar$ we assume the neutron and proton pairing interaction to be zero. The expectation value of the Hamiltonian in eq. (9) is then obtained for the state with angular momentum I corresponding to a sloping Fermi surface ("optimal" configuration) using the wave function $\Psi(\beta_2, \beta_{40}, \gamma, J)$, which is a Slater determinant of the energetically lowest single-particle wave functions. In this way we cannot describe all the angular momenta along the yrast line, and we adopt here the suggestion of the Lund-Warsaw group [5,6]) to construct all states with various angular momenta inbetween the "optimal" states by 1p–1h, 2p–2h excitations over the straight sloping Fermi surface. This is probably adequate provided sufficiently many optimal states are considered. Calculations including 3p–3h and higher configurations have been made in a cranked single-particle potential, and no case has ever been found where such a state is yrast. States obtained in such a way are therefore given by the Slater determinant of the "nearest" "optimal" state modified by the exchange of one (two) nucleonic wave function(s) below the Fermi surface by one (two) s.p. wave function(s) from above.

As the inert core in our calculations we choose the nucleus $^{110}_{40}Zr_{70}$. The Coulomb energy term is calculated for the homogeneously charged drop with a shape parametrized by the quadrupole β_2 and γ and hexadecapole β_{40} deformations [18]). The addition of the Coulomb energy to the expectation value of the many-body Hamiltonian (7) increases the ground-state (g.s.) deformation over the values deduced from the experiments. We believe that the best choice of the force parameters entering the Hamiltonian (7) can be obtained by fitting them to the experimentally measured

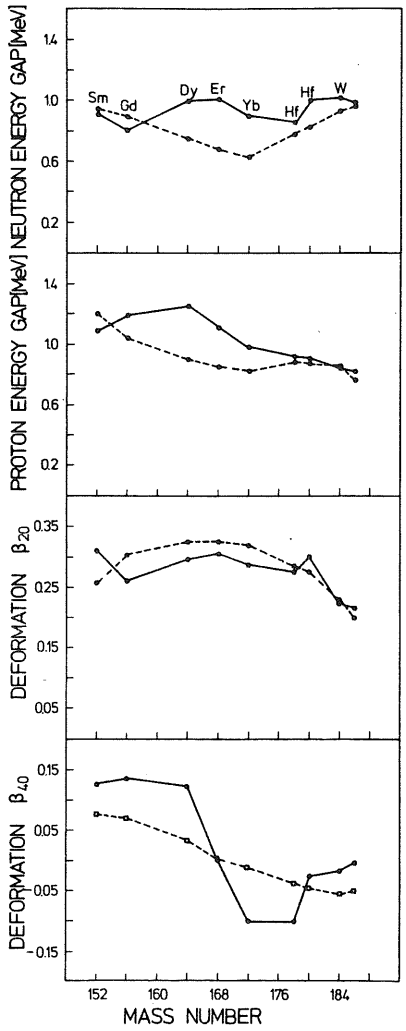

Fig. 1. Quadrupole β_{20} and hexadecapole β_{40} deformations as well as the proton and neutron energy gaps obtained for several rare-earth nuclei by minimising the total energy (10) for $I = 0$ with the force strength parameters given in table 1 (solid lines). The dashed lines with open circles represent the odd-even mass differences and the quadrupole deformations obtained in the P+QQ model [15]). The experimental hexadecapole deformations are given here by the open squares.

TABLE 1

The force strength parameters

Mass	χ_{20}	χ_{40}	G_{p0}	G_{n0}
A = 148–168	65	50	25	20
A = 168–188	69	80	23	18

deformations β_2 and β_{40} and the energy gaps Δ_p and Δ_n. The A-dependence of the pairing forces G_n and G_p as well as that of the quadrupole force χ_2 has been taken from Kumar and Baranger [15])

$$\chi_2 = \chi_{20} A^{-1.4},$$

$$G_\tau = G_{\tau_0} A^{-1},$$

and the constants χ_{20} and G_{τ_0} have been fitted in order to reproduce the measured g.s. properties. The schematic hexadecapole force used has the same r^2 dependence as that of the quadrupole forces. Therefore it is reasonable to assume also the same A-dependence for the $Y_{4\mu} \times Y_{4\mu}$ forces. The discrepancy between the hexadecapole force used and the $Y_{4\mu}$ component of the realistic two-body forces can be removed by choosing a different constant χ_4 for different parts of the rare-earth region. In fig. 1 the results are shown for the deformations β_2 and β_{40} as well as for the proton and neutron energy gaps obtained by minimising the total energy expression (10) for $J = 0$. The best choice of the force strength parameters corresponding to the fit shown in fig. 1 is given in table 1.

For the formation of yrast traps it is essential that no collective rotation is possible. Therefore the application of this method will here be restricted to nuclei for which calculations indicate [4,6,7,9]) that they rotate around the symmetry axis.

The method described in this section is able to describe the yrast traps, if one includes particle-hole excitations across the sloping Fermi surface determined by the cranking term $-\omega j_x$. Up to the particle-hole excitations the method is in principle the same as the one used in ref. [10]). But we have improved the single-particle basis, added a hexadecapole force and readjusted the force parameters to the ground-state properties after extending the Hamiltonian by a Coulomb term and a hexadecapole force.

3. Results and discussion

We have performed the microscopic calculation of the yrast line for $\gamma = -60°$, $\beta_2 \gtrsim 0$ using the model described in sect. 2. We restricted our analysis to those nuclei which in the microscopic calculations of ref. [9]) have the lowest minimum at $\gamma = -60°$ (for the angular momenta between $30\hbar$ and $70\hbar$). We did not check the stability of the minimum in the β_2–γ plane with respect to the β_{40} deformation. Only for the neutron deficient light rare-earth nuclei does the lowest minimum have $\gamma = -60°$ for angular momenta between $30\hbar$ and $70\hbar$. This result agrees with the predictions of the semi-microscopic calculations of refs. [3–7]). In figs. 2–4 the energy surfaces of $^{148}_{62}Sm_{86}$, $^{150}_{64}Gd_{86}$ and $^{158}_{70}Yb_{88}$ obtained microscopically using the approach of ref. [9]) are shown as a function of β_2 and γ deformations for angular momenta $I = 30\hbar$, $50\hbar$, $70\hbar$ and $80\hbar$. The energy difference between the equi-energy lines is 1 MeV. The shaded areas in figs. 2–4 represent the points in the β_2–γ plane with the

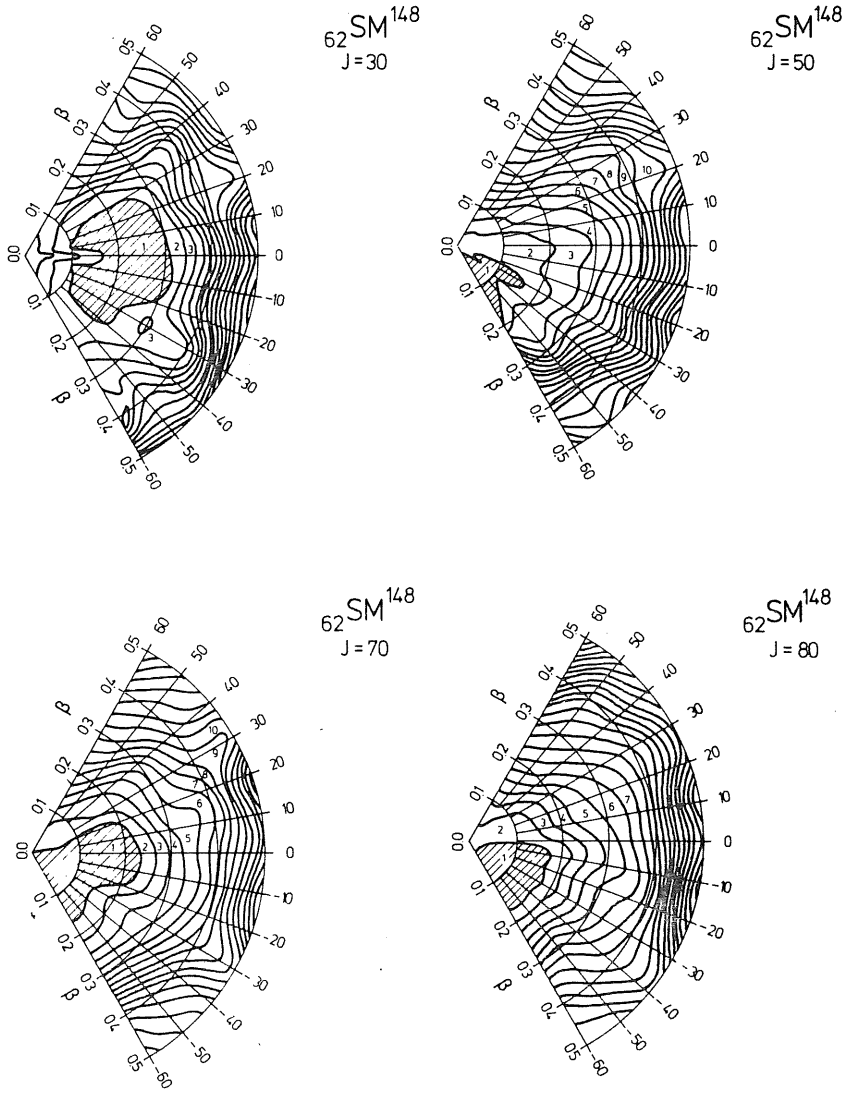

Fig. 2. The deformation energy surfaces obtained for $^{148}_{62}$Sm by minimising the total energy (10) for angular momenta $I = 30\hbar$, $50\hbar$, $70\hbar$ and $80\hbar$. The shaded areas represent the lowest minimum of the energy. The energy difference between the equi-energy lines is 1 MeV. The predictions of our model concerning the position of the lowest minimum can be more trusted up to the angular momentum $I \approx 70\hbar$. Above $I \gtrsim 70\hbar$ the average moment of inertia $\tilde{J} = \tilde{I}/\omega_{\mathrm{rot}}$ in a microscopic method has an unproper asymptotic value [9]). This can result in a systematic error for the energy of the yrast states.

excitation energy (relative to the absolute minimum) not more than 1 MeV. The strength of the quadrupole-quadrupole force used is $\chi_2 = 65A^{-1.4}$ [MeV]. In $^{148}_{62}\mathrm{Sm}_{86}$ the lowest minimum for $I = 30\hbar$ corresponds to $\gamma \approx 0°$. With increase of the angular momenta this minimum moves towards the $\gamma = -60°$ line and at around

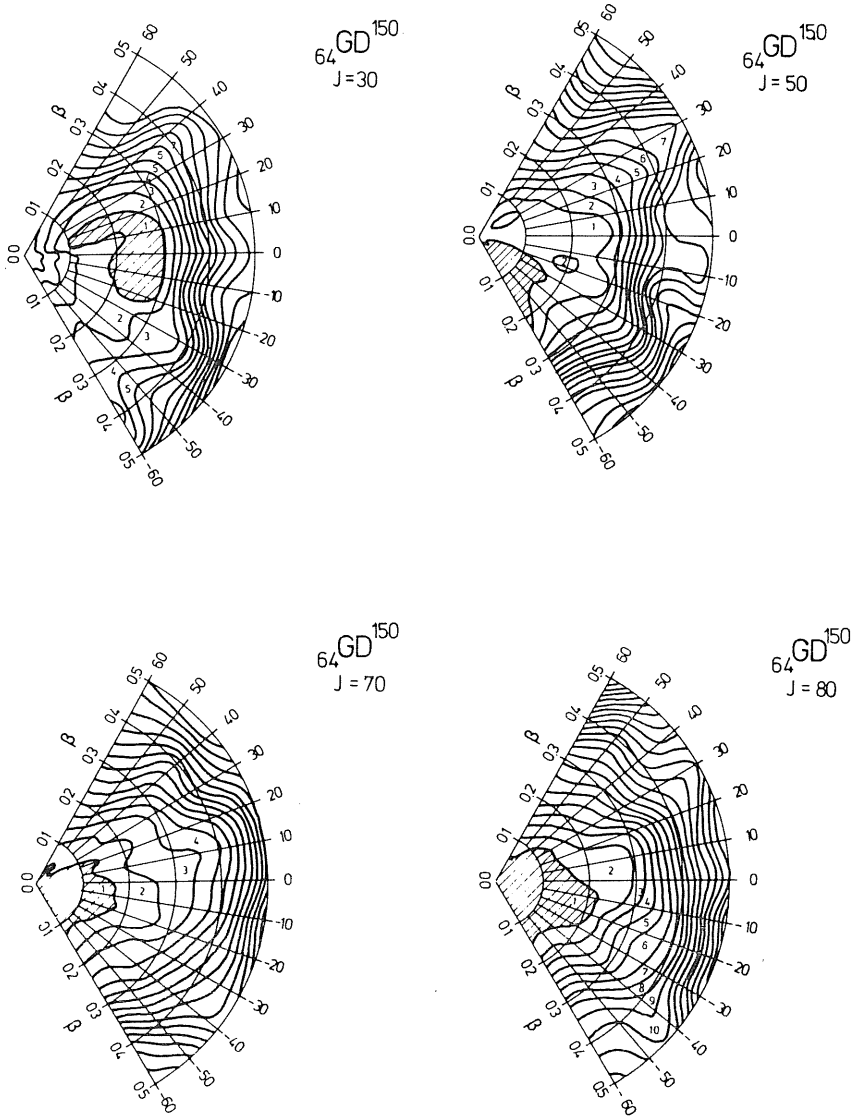

Fig. 3. The deformation energy surfaces obtained for $^{150}_{64}$Gd for angular momenta $I = 30\hbar$, $50\hbar$, $70\hbar$ and $80\hbar$. For details see caption of fig. 2.

$I = 50\hbar$ the absolute minimum has $\gamma = -60°$ (oblate shape rotating around the symmetry axis). The deformation energy surface close to minimum point is very flat and, therefore, one expects the correlated wave function of the system to be spread over a large range of deformations. For angular momenta $I = 30$–$50\hbar$ one may find a finite shrinking from the deformation $\beta_2 \approx 0.2$ at $I = 30\hbar$ to $\beta_2 \approx 0.1$ at

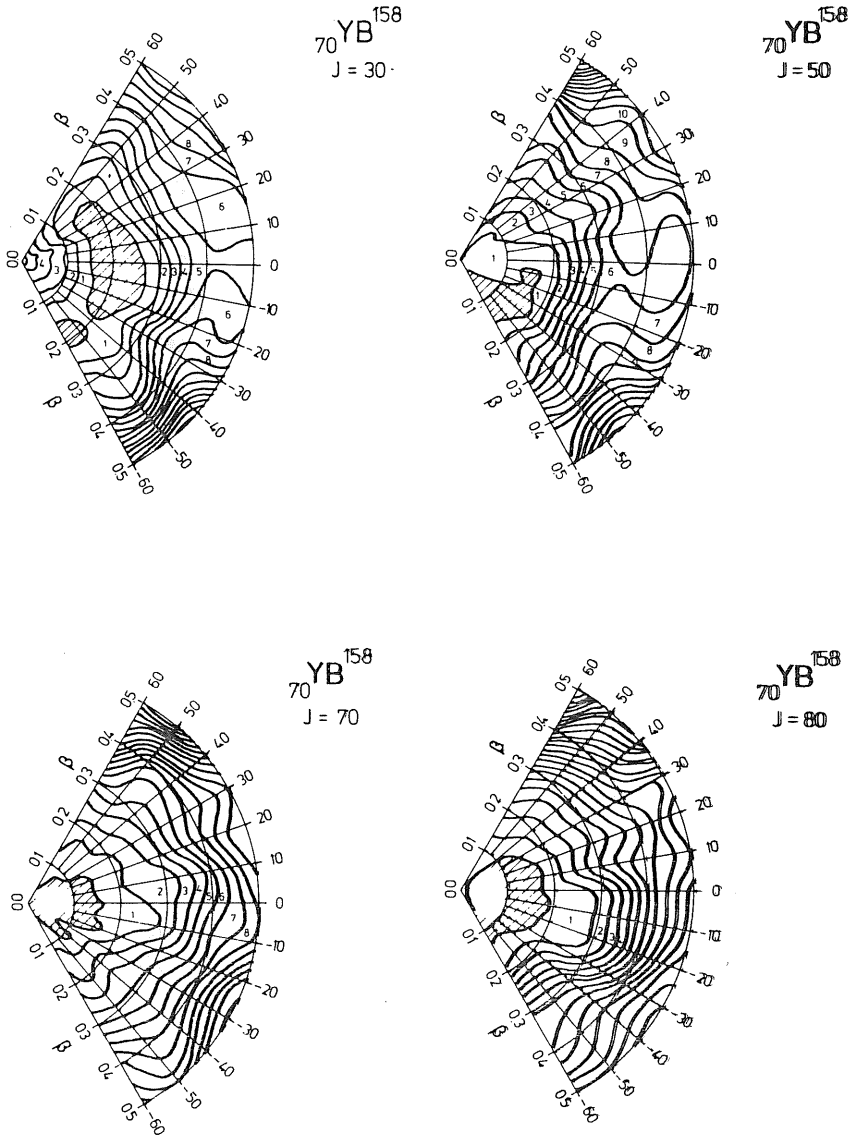

Fig. 4. The deformation energy surfaces obtained for $^{158}_{70}$Yb for angular momenta $I = 30\hbar$, $50\hbar$, $70\hbar$ and $80\hbar$. For details see caption of fig. 2.

$I = 50\hbar$. The situation is very much the same for $^{150}_{64}Gd_{86}$ (see fig. 3) which suggests the dominant role of neutrons in the qualitative behaviour of the energy landscapes at very high spins in the light, neutron deficient rare-earth nuclei. The energy landscape for $^{158}_{70}$Yb is shown in fig. 4. Here we have a local minimum at

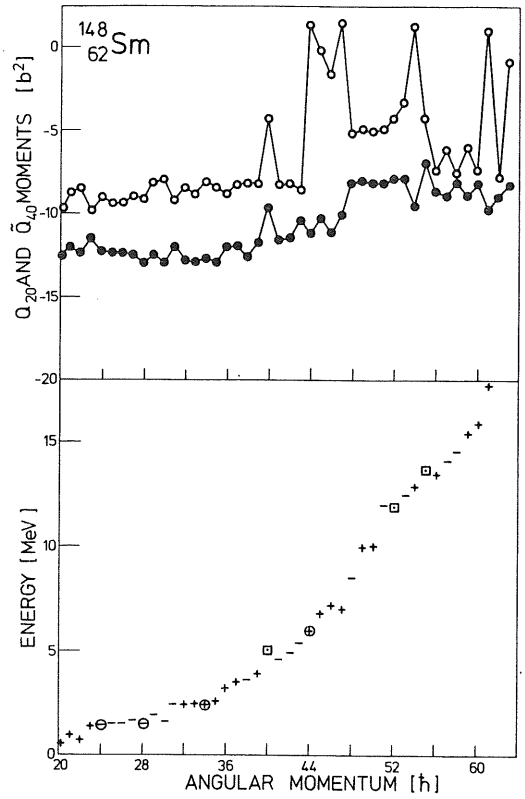

Fig. 5. The excitation energies as well as the quadrupole Q_{20} (solid circles) and the hexadecapole $\tilde{Q}_{40}$ moments (open circles) of the yrast states are shown as a function of the total angular momentum for $^{148}_{62}$Sm. The yrast traps are marked by encircled "+" or "−" where +(−) denotes the positive-(negative-) parity states. The points in squares correspond to the "optimal" configuration.

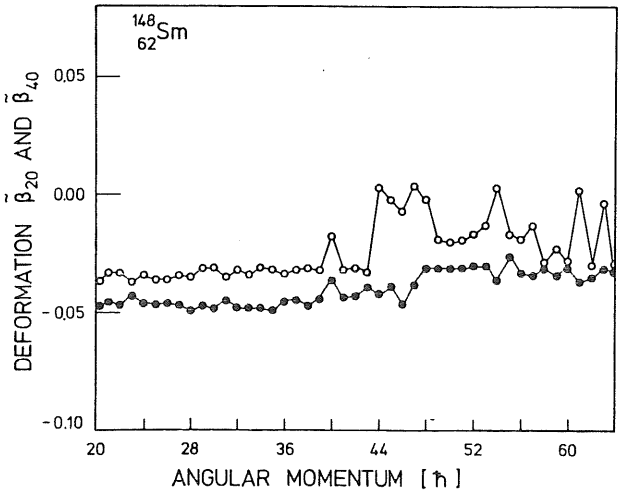

Fig. 6. The quadrupole β_{20} (closed circles) and hexadecapole β_{40} (open circles) deformations of the yrast states for $^{148}_{62}$Sm are obtained from the calculated Q_{20} and $\tilde{Q}_{40}$ moments assuming the sharp cutoff model for the nuclear density.

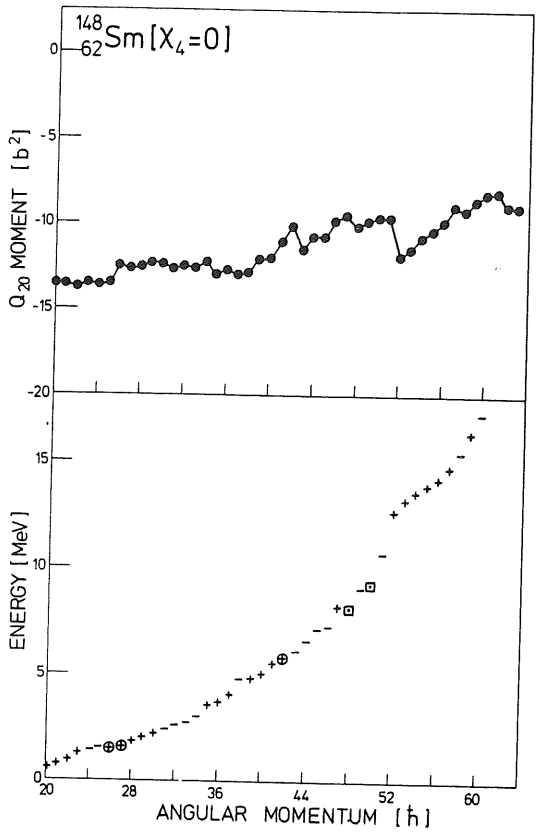

Fig. 7. The excitation energies and the quadrupole moments (solid circles) of the yrast states are shown as a function of the total angular momentum for $^{148}_{62}$Sm. The results have been obtained without the hexadecapole term in the trial wave function and in the many-body Hamiltonian. The yrast traps are marked by encircled "+" or "−" where +(−) denotes the positive- (negative-) parity states. The points in squares correspond to the "optimal" configuration.

$\gamma = -60°$ already for the angular momentum $I = 30\hbar$. This minimum is the lowest for $I = 50\hbar$. The nucleus $^{158}_{70}Yb_{88}$ seems to be most adequate for our analysis since it exhibits the local minimum at $\gamma = -60°$ for $I = 30$–$70\hbar$. As representatives of the light rare-earth nuclei we have chosen ^{148}Sm, ^{150}Gd and ^{158}Yb for the calculations.

The results for ^{148}Sm are shown in figs. 5–7. In fig. 5 the excitation energies as well as the quadrupole Q_{20} and hexadecapole $\tilde{Q}_{40}$ moments of the yrast states versus the total angular momentum are given. As in ref. [6]), we define the traps as yrast states which cannot undergo γ-decay by an E1, M1, E2 or M2 transition. The traps are marked by encircled "+" or "−" where + (−) denotes the positive (negative) parity states. The points in squares correspond to the "optimal configuration". The solid circles mark the quadrupole moment of the yrast state and the open circles depict the hexadecapole moment. The results presented in fig. 5 have been

obtained using the trial wave function calculated for the selected set of deformations, viz. $\beta_2 = 0.05$, 0.10, 0.15, 0.20, 0.25 and 0.30, $\beta_{40} = -0.15$, -0.10, -0.05, 0.0, 0.05, 0.10 and 0.15 and $\gamma = -60°$. We have in this nucleus negative-parity yrast traps with $J^\pi = 24^-$ and 28^- and positive-parity traps with $J^\pi = 34^+$ and 44^+. One cannot, however, exclude that α-particle emission from the isomeric state, which in this region of angular momenta is expected to be quite important [19]), may be comparable to the α-particle emission from other states and it may be difficult to detect delayed γ-rays. The isomerism in the state of $J^\pi = 44^+$ is connected with a drastic change of the hexadecapole $\tilde{Q}_{40}$ moment going from the states 43^- to 44^- (from -10 b^2 for $J = 43^-$ to zero for $J = 44^+$). This change in $\tilde{Q}_{40}$ value leads to a disappearance of the hexadecapole correlation energy for the $J^\pi = 44^+$. The variations of the hexadecapole moment in fig. 5 starting above the angular momentum $43\hbar$ are of interest. It seems that there are two competing minima in the β_{40} direction at $\beta_{40} = 0$ $\beta_{40} \approx -0.035$ (see fig. 6). The variation of the quadrupole moment is of little significance. This can be clearly seen in fig. 6 where the quadrupole β_2 and hexadecapole β_{40} deformations are shown. They are obtained from the calculated Q_{20} and $\tilde{Q}_{40}$ moments assuming a homogeneous matter distribution.

In fig. 7 the excitation energies as well as the quadrupole moments of the yrast states are shown, which have been calculated using the total energy expression (10) with no hexadecapole force term ($\chi_4 = 0$). The strength β_2 of the quadrupole force is taken from ref. [9]) and is the same in all the calculations reported here ($\chi = 65 \times A^{-1.4}$ MeV). Comparing figs. 5 and 7 one does not see any correlations between the positions of the yrast levels calculated with and without the hexadecapole force. In fig. 7 we have three isomeric states for $J = 26$, 27 and 42, all of them with positive parity. They are isomeric because they are different by more than 1p–1h excitations from the states with $J-1$ and $J-2$.

The results for $^{150}_{64}$Gd are shown in figs. 8–10. In fig. 8 the excitation energies, quadrupole and hexadecapole moments of the yrast states obtained using definition (7) are shown. One should mention that the traps at $J^\pi = 23^-$ and $J^\pi = 31^+$ have about 1 MeV smaller excitation energies than the states with two units of angular momentum less, and therefore they should decay exclusively by higher multipoles. Moreover, such a large energy difference (1 MeV) guarantees that the effects not included in our model (like the pairing correlations) will not change the results. In ^{150}Gd similar to the case of $^{148}_{62}$Sm one may also see the drastic variation of the hexadecapole deformation with the angular momentum (see fig. 10). These variations start here already at $J = 27$. The excitation energies and quadrupole moments of the yrast states calculated for $\chi_4 = 0$ are once more very different as compared to the yrast energies and quadrupole moments obtained with $\chi_4 \neq 0$. The yrast traps for $J^\pi = 21^-$, 22^-, 24^+, 26^+ and 36^+ (see fig. 8) cannot decay by γ-rays due to the 1p–1h nature of the transition operator. The quadrupole moment is a rapidly changing function of the total angular momenta.

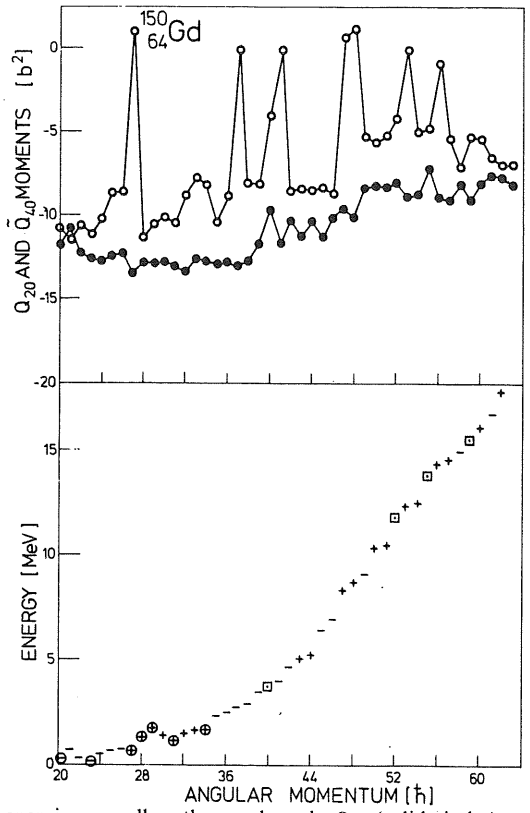

Fig. 8. The excitation energies as well as the quadrupole Q_{20} (solid circles) and the hexadecapole $\tilde{Q}_{40}$ moments (open circles) of the yrast states are shown as a function of the total angular momentum for $^{150}_{64}$Gd. For details see caption of fig. 5.

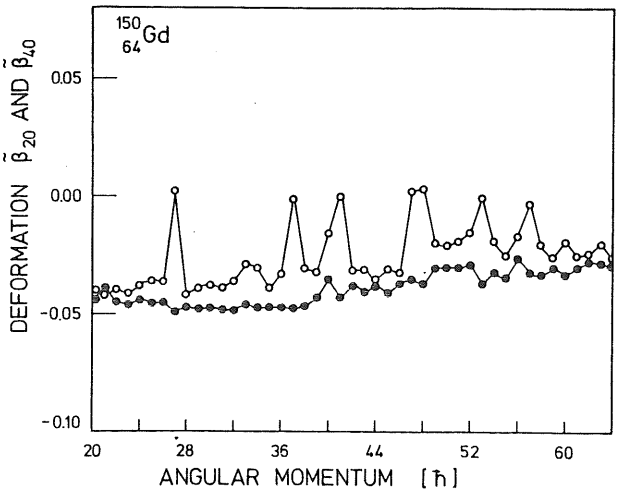

Fig. 9. The quadrupole β_{20} (closed circles) and hexadecapole β_{40} (open circles) deformations of the yrast states are shown as a function of the total angular momentum for $^{150}_{64}$Gd. For details see caption of fig. 6.

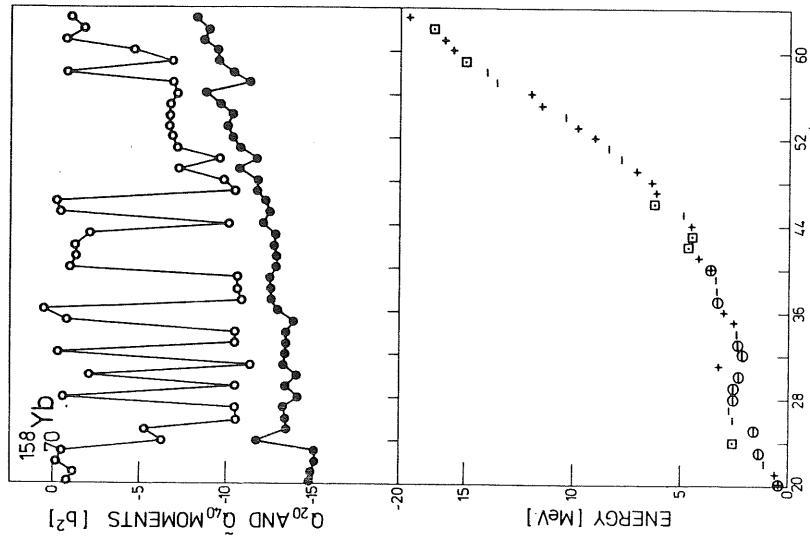

Fig. 11. The excitation energies as well as the quadrupole Q_{20} (solid circles) and the hexadecapole $\tilde{Q}_{40}$ moments (open circles) of the yrast states are shown as a function of the total angular momentum for $^{158}_{70}$Yb. For details see caption of fig. 5.

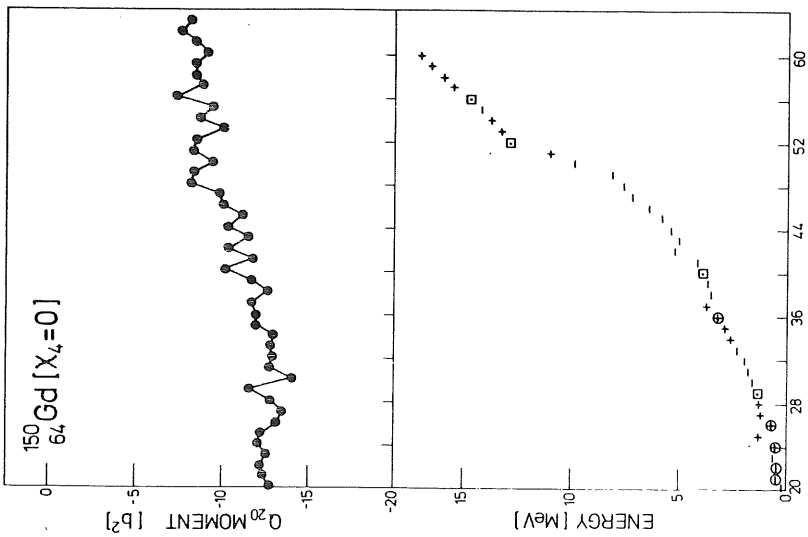

Fig. 10. The excitation energies and the quadrupole moments (solid circles) of the yrast states are shown as a function of the total angular momentum for $^{150}_{64}$Gd. For details see caption of fig. 7.

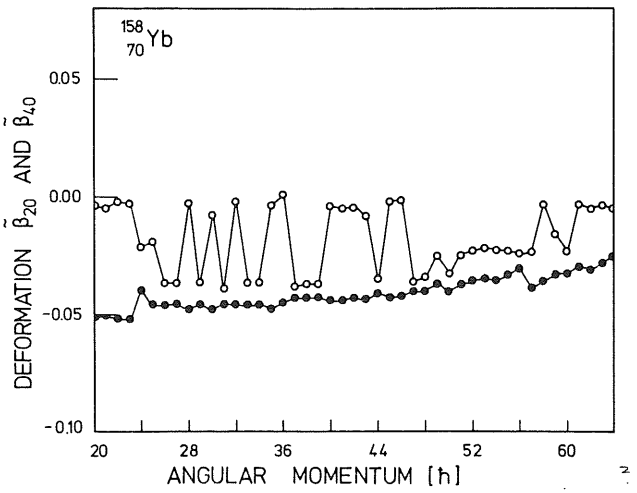

Fig. 12. The quadrupole β_{20} (closed circles) and hexadecapole β_{40} (open circles) deformations of the yrast states are shown as a function of the total angular momentum for $^{158}_{70}$Yb. For details see caption of fig. 6.

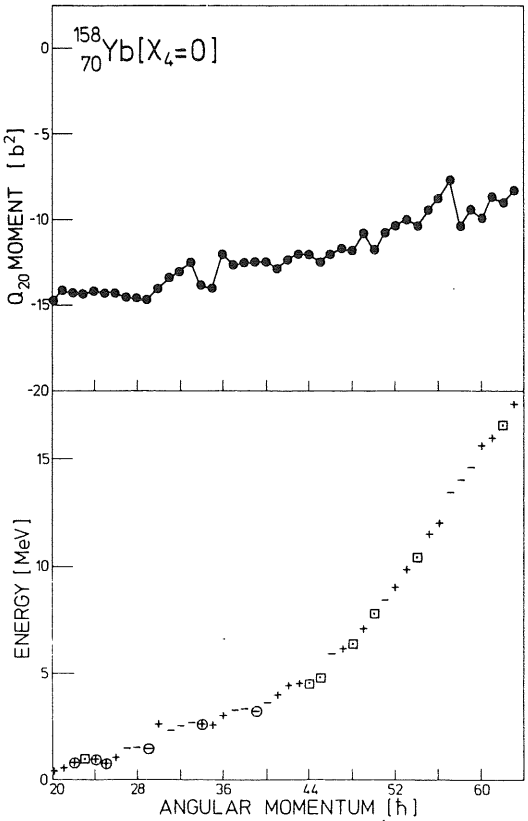

Fig. 13. The excitation energies and the quadrupole moments (solid circles) of the yrast states are shown as a function of the total angular momentum for $^{158}_{70}$Yb. For details see caption of fig. 7.

Last, the results for the nucleus $^{158}_{70}Yb_{88}$ are presented in figs. 11–13. The characteristic features of the results are the very large changes in the hexadecapole deformation above $J = 24$. Such a series of the yrast traps as $J^{\pi} = 23^{-}, 25^{-}, 28^{-}, 29^{-}, 30^{-}, 32^{-}$ and 33^{-} is formed due to the variation in the hexadecapole deformation from 0 to -0.04. (The deformation parameters are calculated assuming a homogeneous matter distribution.) The quadrupole deformation is here a very smooth function of the total angular momentum. The structure of the yrast line changes drastically if the hexadecapole force is switched off.

4. Conclusions

The method presented in this paper describes microscopically the formation of yrast traps at very high spin states. An important mechanism which prefers the rotation around a symmetry axis is the MONA effect [10]) (MONA is the maximisation of the overlap of nucleonic wave functions by alignment). Slightly above closed shell nuclei (neutron number 82) this effect seems to stabilize a rotation around the oblate symmetry axis with a small deformation. This is connected with the fact that at the lower end of a shell the large j-levels are concentrated and that for negative deformations the high spin projections Ω are lowered [12]).

In general, we can say that the MONA effect [10]) is responsible for the rotation around a symmetry axis. At the beginning of a shell MONA concentrates the particles near the equator, favours a rotation around an oblate symmetry axis, and alignes the single-particle angular momenta. At the end of the shell MONA bunches the holes near the waist of the nucleus and therefore it prefers rotation around a prolate symmetry axis.

It turns out that traps above angular momentum $I = 40\hbar$ are rather infrequent. This is probably due to the large slope of the yrast line above $I = 40\hbar$, which reduces the importance of the shell fluctuations. Andersson *et al.* [6]) have found traps only up to $30\hbar$. This difference is probably due to the fact that they used the MO single-particle model which, in contrast to the model of Kumar and Baranger, gives too large a slope in the total angular momentum as a function of the cranking frequency. It may also be because with the MO potential the light neutron deficient rare earth nuclei, discussed here, are predicted to become oblate at lower spins.

Last but not least these calculations demonstrate the importance of hexadecapole deformations in the trial wave function and of a hexadecapole force in the residual interaction. The detailed location and structure of the yrast traps are changed in all instances. Therefore it seems that the results of the semi-phenomenological Strutinsky calculations for the deformation energy surfaces using either MO or Woods-Saxon potentials [3–7]) would be significantly modified by including hexadecapole deformations.

Searching for experimental yrast traps guided by calculations like this, one should not forget the following points: (i) Deviations from or even oscillations around

$\gamma = -60°$ reduce the probability for yrast traps. (ii) Configuration mixing will also eliminate some of them. (iii) Particle, especially α-particle, decay may in some cases be faster than the γ-transitions studied here. Thus at the present stage calculations should guide the experimentalist only in the selection of the final nucleus. It seems that the theory can reliably predict if a nucleus has a tendency to rotate around the symmetry axis and thus to produce yrast traps or not.

References

1) S. Cohen, F. Plasil and W. J. Swiatecki, Ann. of Phys. **82** (1974) 557
2) A. Bohr and B. R. Mottelson, Physica Scripta **10A** (1974) 13
3) K. Neergard and V. V. Pashkevich, Phys. Lett. **59B** (1975) 218
4) K. Neergard, V. V. Pashkevich and S. Frauendorf, Nucl. Phys. **A262** (1976) 61
5) R. Bengtsson, S. E. Larsson, G. Leander, P. Möller, S. G. Nilsson, S. Åberg and Z. Szymanski, Phys. Lett. **57B** (1975) 301
6) G. Andersson, R. Bengtsson, S. E. Larsson, G. Leander, P. Möller, S. G. Nilsson, I. Ragnarsson, S. Åberg, J. Dudek, B. Nerlo-Pomorska, K. Pomorski and Z. Szymanski, Nucl. Phys. **A268** (1976) 205
7) K. Neergard, H. Toki, M. Ploszajczak and A. Faessler, Nucl. Phys. **A287** (1977) 48
8) A. Faessler, K. R. Sandhya Devi, F. Grümmer, K. W. Schmid and R. R. Hilton, Nucl. Phys. **A256** (1976) 106
9) M. Ploszajczak, K. R. Sandhya Devi, A. Faessler, Z. Phys., to be published
10) A. Faessler, M. Ploszajczak, K. R. Sandhya Devi, Phys. Rev. Lett. **36** (1976) 1028
11) J. P. Schiffer, Ann. of Phys. **66** (1971) 798;
A. Molinari, M. B. Johnson, H. A. Bethe and W. M. Alberico, Nucl. Phys. **A239** (1975) 45
12) T. Døssing, K. Neergård, K. Matsuyanagi and Hsi-Chen Chang, Phys. Rev. Lett. **39** (1977) 1395
13) A. L. Goodman, Nucl. Phys. **A230** (1974) 466
14) S. G. Nilsson, C. F. Tsang, A. Sobiczewski, Z. Szymanski, S. Wycech, Ch. Gustafson, I. Lamm, P. Möller and B. Nilsson, Nucl. Phys. **A131** (1969) 1
15) K. Kumar and M. Baranger, Nucl. Phys. **A110** (1968) 490, 529
16) S. G. Nilsson, Mat. Fys. Medd. Dan. Vid. Selsk. **29**, no. 16 (1955)
17) W. H. Bassichis, Phys. Rev. **C8** (1973) 480
18) G. Leander, Nucl. Phys. **A219** (1974) 245
19) T. Døssing, S. Frauendorf and H. Schulz, Nucl. Phys. **A287** (1977) 137